*Applied Sciences, Computing and Energy, 2025, 2(2), 323-335*

# Computational Design of Dibenzo[a,c]quinoxalino(2,3-i)phenazine as Eco-Friendly Corrosion Inhibitors: A DFT and Monte Carlo Simulations-Based Study

**Babatunde T. Ogunyemi[1]* and Olawale M. Akinlosotu**
**Received: 22 December 2024/Accepted: 28 March 2025/Published: 04 April 2025**

***Abstract:*** *Corrosion of mild steel in acidic environments remains a critical challenge for industrial infrastructure, driving the need for sustainable, high-performance inhibitors. This study investigates the corrosion-inhibition potential of dibenzo[a,c]quinoxalino(2,3-i)phenazine (DQP), a nitrogen-rich heterocyclic compound, using computational approaches. Density Functional Theory (DFT) and Monte Carlo (MC) simulations were employed to elucidate molecular geometry, electronic properties, and adsorption mechanisms on Fe(110) surfaces. The optimized planar DQP structure exhibits a conjugated π-system with a narrow HOMO-LUMO energy gap (2.48 eV), low chemical hardness (1.24 eV), and high softness (0.806 $eV^{-1}$), indicative of strong electron-donating and accepting capabilities. Fukui function analysis identified nitrogen atoms and adjacent carbons as nucleophilic sites, facilitating multidentate coordination with iron surfaces. Molecular electrostatic potential maps further localized electron-rich regions over nitrogen atoms, corroborating their role in chemisorption. MC simulations revealed thermodynamically stable adsorption of DQP on Fe(110), with a parallel orientation maximizing π-orbital interactions and surface coverage. The negative back-donation energy (-1.11 eV) and low adsorption energy (-50.41 kJ/mol) highlight efficient charge transfer and robust interfacial stability. Electronic absorption spectra highlighted intramolecular charge transfer transitions (419.78–515.48 nm), reinforcing DQP's capacity to passivate metal surfaces. The dual functionality of DQP (electron donation via heteroatoms and electron acceptance through back-donation) alongside its planar adsorption geometry, positions it as a potent eco-friendly inhibitor. These findings provide a computational framework for rational design of corrosion inhibitors, emphasizing molecular engineering to balance efficacy, stability, and environmental compatibility.*

***Keyword:*** *Corrosion inhibition; Dibenzo[a,c]quinoxalino(2,3-i)phenazine; Density Functional Theory (DFT); Monte Carlo simulations.*

**Babatunde T. Ogunyemi***
Department of Chemistry, Federal University Otuoke, Bayelsa State, Nigeria
**Email:** ogunyemibt@fuotuoke.edu.ng
**Orcid id:0000-0002-3634-488X**

**Olawale M. Akinlosotu**
Department of Chemistry, Federal University Otuoke, Bayelsa State, Nigeria
**Email: oakinlosotu50@gmail.com**

## 1.0 Introduction

Corrosion is a persistent industrial challenge, particularly for infrastructure composed of mild steel exposed to acidic environments. This electrochemical deterioration of metal surfaces not only compromises structural integrity but also imposes substantial economic burdens and environmental risks. The need for effective corrosion mitigation strategies is therefore both urgent and widespread. Conventional corrosion inhibitors—often comprising heavy metals or toxic organic compounds—pose additional concerns due to their adverse ecological and health effects, which contradict global

sustainability goals and stringent environmental regulations (Verma et al., 2021). The search for eco-friendly and sustainable alternatives has led to extensive exploration of green corrosion inhibitors. Natural products, such as plant extracts and biopolymers, have been widely studied due to their biodegradability and low toxicity (Eddy, 2010; Odoemelam et al., 2018; El Nemr et al., 2024). However, these bio-based inhibitors often suffer from variability in composition and performance under different environmental conditions (Eddy et al., 2023). Recent research has also explored plant waste materials (Eddy et al., 2023), neem leaves (Odoemelam et al., 2018), and ethanol extracts from *Garcinia kola*, *Cola nitida*, and *Andrographis paniculata* (Eddy, 2010; Eddy et al., 2011) as promising corrosion-inhibiting agents.

Beyond natural compounds, synthetic corrosion inhibitors, particularly those based on nitrogen-rich heterocyclic molecules, have attracted growing interest due to their ability to form stable chemisorbed layers on metal surfaces through lone pair electron donation and π-interactions (Elsayed et al., 2024; Belal et al., 2023). Polymers and their nanocomposites have also emerged as high-performance coatings that can significantly enhance corrosion resistance and durability (Anjum et al., 2025). Piperazine derivatives (Singaravelu et al., 2024) and imidazotriazole derivatives (Elsayed et al., 2024) further underscore the potential of synthetically tailored compounds for targeted inhibition performance.

One particularly promising synthetic candidate is the class of dibenzo[a,c]quinoxalino(2,3-i)phenazine (DQP) derivatives. With extended π-conjugated systems and multiple nitrogen donor atoms, DQPs possess physicochemical properties conducive to strong adsorption and protective film formation on metal surfaces. Recent experimental studies have reported inhibition efficiencies of over 98% in acidic media for mild steel, highlighting the potential of DQPs as high-performance corrosion inhibitors (Akinlosotu et al., 2023). Despite this, comprehensive theoretical analyses of their adsorption behavior and electronic interactions with metallic surfaces remain limited.

To bridge this knowledge gap, computational chemistry methods, notably Density Functional Theory (DFT) and Monte Carlo (MC) simulations have proven invaluable for elucidating molecular-level interactions, predicting reactivity descriptors, and simulating adsorption mechanisms (Kalajahi et al., 2023; Chang, 2022). DFT provides insight into electron distribution, frontier orbital energies, chemical hardness and softness, and reactivity indices such as the Fukui function. Monte Carlo simulations further model the thermodynamics and spatial configurations of inhibitor adsorption on metal surfaces under realistic conditions.

This study aims to design and evaluate dibenzo[a,c]quinoxalino(2,3-i)phenazine (DQP) as a sustainable, high-performance corrosion inhibitor for mild steel in acidic environments using Density Functional Theory and Monte Carlo simulations. The research investigates the molecular geometry, electronic structure, adsorption mechanisms, and thermodynamic stability of DQP when interfaced with iron surfaces.

The findings from this study will contribute significantly to the rational design of environmentally benign corrosion inhibitors. By uncovering the electronic and structural features that govern inhibitor efficiency, this work offers a computational blueprint for developing next-generation corrosion inhibitors that meet both performance and environmental standards. The dual benefit of computational pre-screening and structural optimization reduces experimental costs and accelerates the transition from theoretical design to industrial application.

## 2. Materials and Methods

### *2.1 Computational Details*

Molecular modeling has emerged as a powerful alternative for interpreting experimental data, particularly when predicting properties of new materials that meet industrial needs. This study employed quantum chemical methods within Spartan 14 package (version 2.4) (Spartan et al., 2013) for all calculations, focusing on an isolated gaseous system at 298.15K and 1 atmosphere pressure. The research involved ground-state geometry optimization and energy calculations for studied molecule using DFT/B3LYP (Becke, 1993: Lee 1988) with the 6-31G(d) basis set (Yang et al., 1998). During optimization, all bond angles, dihedral angles, and bond lengths remained unconstrained to ensure real vibrational frequencies. Calculations included energy levels of molecular orbitals specifically $E_{HOMO}$ and $E_{LUMO}$ to identify key adsorption sites. These frontier orbitals play a crucial role in predicting how organic inhibitors interact with metal surfaces.

The study derived ionization potential (IP) and electron affinity (EA) for all inhibitors from their HOMO and LUMO energies using Koopman's theorem (Pearson et al., 1988), as shown below:

$$IP = -E_{HOMO} \quad (1)$$

$$EA = -E_{LUMO} \quad (2)$$

The calculations for absolute hardness and electronegativity (χ) values used the following formulas:

$$\eta = \left(\frac{\delta\varepsilon^2}{\delta N^2}\right)_{v(r)} = \frac{E_{LUMO} + E_{HOMO}}{2} = \frac{IP - EA}{2} \quad (3)$$

$$\chi = -\mu = \left(\frac{\delta\varepsilon}{\delta N}\right)_{v(r)} = -\frac{E_{LUMO} + E_{HOMO}}{2} = \frac{IP + EA}{2} \quad (4)$$

The softness (S), which is the inverse of hardness, was determined through:

$$S = \frac{1}{\eta} \quad (5)$$

These quantum parameters are essential in evaluating the chemical reactivity of organic inhibitors.

When metal contacts an organic molecule, electrons flow between systems until their chemical potentials align. The number of transferred electrons (ΔN) was calculated as reported by Parr et al. (1983):

$$\Delta N = \frac{\chi_{Fe} - \chi_{inh}}{2(\eta_{Fe} + \eta_{inh})} \quad (6)$$

where $\chi_{Fe}$ and $\chi_{inh}$ represent the absolute electronegativities of iron (Fe) and organic inhibitor respectively. while $\eta_{Fe}$ and $\eta_{inh}$ represent their hardness. For iron, theoretical values of $\chi_{Fe} = 7$ eV/mole and $\eta_{Fe} = 0\ eV/mole$ (Pearson 1988: Ogunyemi, *et al.,* 2020) were employed to estimate the electron transfer**.**

Back-donation charges, a crucial parameter for understanding charge redistribution was calculated using using:

$$\Delta E_{(Back-donation)} = \frac{\mu}{4} \quad (7)$$

Additionally, the study evaluated the electrophilicity index (ω) of each molecular inhibitor through the following equation (Parr et al., 1999):

$$\omega = \frac{\mu^2}{2\eta} \quad (8)$$

A lower μ and ω indicates a more reactive nucleophile, while higher values suggest an active electrophile.

Local reactivity was assessed through Fukui indices, computed via Mulliken population analysis of neutral, cationic, and anionic species. using the optimized geometries. Condensed Fukui functions for nucleophilic ($f_k^+$) and electrophilic ($f_k^-$) attacks were computed based on the Mulliken population

analysis. The partial atomic charge is defined by $q_k(N+1)$ when a molecule accepts electron and by $q_k(N-1)$ when it loses an electron. For a neutral molecule, the charge on each atom is defined by $q_k(N)$The nucleophilic, electrophilic and dual Fukui parameters were calculated using Yao's dual descriptors as shown in Eqs. 8, 9 and 10, respectively.

$$f_k^+ = [q_k(N+1) - q_k(N)]$$
nucleophilic attack (9)

$$f_k^- = [q_k(N) - q_k(N-1)]$$
electrophilic attack (10)

$$\Delta f_k(r) = f_k^+ - f_k^- \quad (11)$$

These indices pinpointed regions prone to nucleophilic or electrophilic interactions and offers insights into potential binding sites. Molecular electrostatic potential (MEP) maps further visualized charge distribution, highlighting areas likely to engage with iron surfaces (Eddy *et al*., 2010).

### *2.2 Monte Carlo Simulation*

Monte Carlo (MC) simulations assessed adsorption and simulated possible interactions between inhibitors and iron surface, specifically between inhibitor molecules and Fe(110) surface along low-index miller facet for stable iron plane. The selection of Fe(110) plane was based on reports of its good stability and well-packed structure (Kabanda et al., 2013; Farhadian et al., 2021 32). The Forcite module achieved full geometry optimization of the studied molecule. The model used a Fe(110) surface as a 10×10 supercell with vacuum thickness of 30 Å and box volume/cell volume of 6. Five annealing cycles with 50,000 steps per cycle were applied for fine-quality adsorption calculations using simulated annealing (Oyeneyin,et al., 2021). This approach obtained and reported the low-energy configurations of the Fe(110)-inhibitor system in aqueous medium. To reflect real-life corrosion processes, the MC simulation included water molecules and HCl environment. The study examined adsorption of inhibitors on Fe(110) surface using condensed phase optimized molecular potentials for atomistic simulation studies (COMPASS) force field in the adsorption locator module. Calculations determined adsorption energy as the sum of the rigid adsorption energy (E) and the deformation energy (E) in kcal/mol (Verma et al.,2021; Oyeneyin et al., 2021). The Forcite and Adsorption Locator modules in Materials Studio 2017 software facilitated the MC simulations.

## 3.0 Results and Discussion

### *3.1 Molecular Geometry of Dibenzo [a,c[quinoxalino(2,3-i)phenazine(DQP)*

The optimized geometry (Figure 1) and dihedral angles (Table 1) of Dibenzo [a,c[quinoxalino(2,3-i)phenazine reveal a fully planar structure, with all listed dihedral angles at 180°. This planarity is characteristic of conjugated π-systems, which enhance electronic delocalization and thermodynamic stability. The rigid, fused aromatic framework suggests strong intramolecular charge transfer (ICT) capabilities, critical for applications in organic electronics or photovoltaics. The absence of steric distortion aligns with similar polycyclic aromatic hydrocarbons (PAHs), where planarity maximizes π-orbital overlap, reducing energy gaps and facilitating electron mobility.

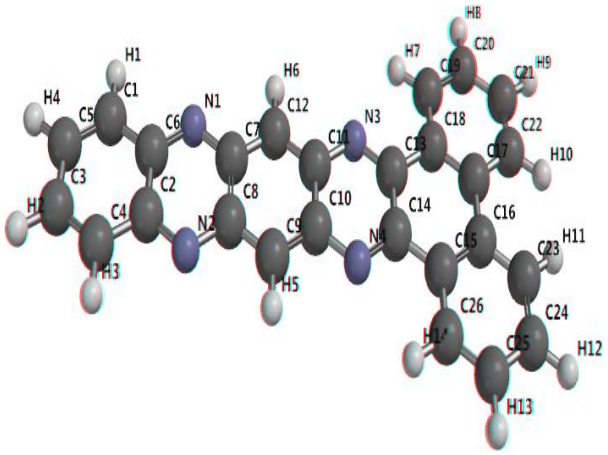


**Fig. 1: Optimized geometry of Dibenzo [a,c[quinoxalino(2,3-i)phenazine**

**Table 1: Dihedral Angle of Dibenzo [a,c[quinoxalino(2,3-i)phenazine**

| Dibenzo [a,c[quinoxalino(2,3-i)phenazine | Dihedral Angle(º) |
|---|---|
| $C_5C_1C_6N_1$ | 180.00 |
| $C_8N_1C_7C_{12}$ | 180.00 |
| $C_{12}C_{11}N_3C_{13}$ | 180.00 |
| $C_{11}N_3C_{13}C_{18}$ | 180.00 |
| $C_3C_4C_2N_2$ | 180.00 |
| $C_2N_2C_8C_9$ | 180.00 |
| $C_9C_{10}N_4C_{14}$ | 180.00 |
| $C_{10}N_4C_{14}C_{15}$ | 180.00 |

### *3.2 Quantum Chemical and Global Reactivity Descriptors of DQP*

The quantum chemical and global reactivity descriptors (Table 2) of dibenzo[a,c]quinoxalino(2,3-i) phenazine (DQP) were systematically evaluated using density functional theory (DFT) to elucidate its potential as a corrosion inhibitor. The HOMO energy ($E_{HOMO}$: -5.68 eV) and LUMO energy ($E_{LUMO}$: -3.2 eV) provide insight into the molecule's electron-donating and accepting capabilities, respectively. A narrow energy gap (ΔE: 2.48 eV) suggests enhanced reactivity, a hallmark of effective inhibitors, as lower bandgap molecules often exhibit stronger adsorption on metallic surfaces (Obot et al., 2015; Ogunyemi et al., 2020). The derived chemical hardness (η: 1.24 eV) and softness (S: 0.806 $eV^{-1}$) further corroborate the molecular softness, aligning with the propensity of soft molecules to facilitate charge transfer interactions with metal substrates (Pearson, 1997).

The calculated number of electron transfers (ΔN: 1.03) indicates a moderate electron-donating tendency, which is critical for forming protective chemisorbed layers on metal surfaces. Hydrophobicity, quantified by Log P (2.43), suggests sufficient lipophilicity to facilitate adsorption, while the polar surface area (PSA: 73.32 Å²) reflects a balance between solubility and interfacial interactions. The solvation energy ($E_{solv}$: -50.41 kJ/mol) underscores the thermodynamic stability of DQP in aqueous environments, a prerequisite for practical inhibitor applications (Tomasi et al., 2005). Additionally, the ionization

potential (IP: 5.68 eV) and electron affinity (EA: 3.2 eV) yield an electronegativity (χ: 4.44) and electrophilicity index (ω: 7.949), parameters that collectively describe the molecule's capacity to participate in electrophilic and nucleophilic interactions, essential for binding to corroding metal surfaces (Parr et al., 1999).

The molecular volume (V = 382.19 Å$^3$) and low dipole moment (DM = 1 debye) suggest a compact yet polarizable structure, facilitating both adsorption and coverage efficiency. Notably, the negative back-donation energy ($\Delta E_{back\text{-}donation}$: -1.11 eV) implies stabilization through electron back-donation from metal d-orbitals to the inhibitor's antibonding orbitals, a mechanism often associated with enhanced inhibition efficiency.

**Table 2: Quantum chemical and global reactivity descriptors of DQP**

| Quantum descriptors | QDP |
|---|---|
| **$E_{HOMO}$ (eV)** | -5.68 |
| **$E_{LUMO}$ (eV)** | -3.2 |
| **ΔE (eV)** | 2.48 |
| ***η* (eV)** | 1.24 |
| ***S*(eV$^{-1}$)** | 0.806 |
| **ΔN** | 1.032 |
| **Log P** | 2.43 |
| **Ovality** | 1.47 |
| **PSA** | 73.32 |
| **Polarizability** | 71.77 |
| **$E_{solv\ (kJ/mol)}$** | -50.41 |
| **IP** | 5.68 |
| **EA** | 3.2 |
| ***X*** | 4.44 |
| ***Ω*** | 7.949 |
| **V** | 382.19 |
| ***DM (debye)*** | 1 |
| **$\Delta E_{\ back\text{-}donation}$** | -1.11 |
| **MW (amu)** | 117.1 |
| **Energy (au)** | -437.09 |

Figure 2 shows the asymmetrical HOMO-LUMO distribution localized over nitrogen and aromatic regions. this highlight QDP's dual functionality of QDP as an electron donor and acceptor, optimizing its adsorption and corrosion-inhibiting performance.

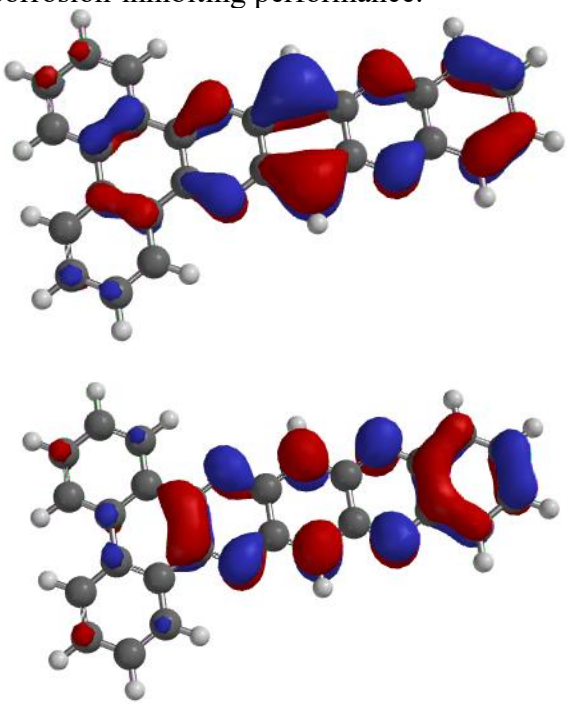

**Fig. 2: Frontier molecular orbitals (FMO) of DQP, calculated at B3LYP/6–31G level of theory.**

### *3.3 Local Reactivity and Adsorption Mechanisms of DQP*

The Fukui indices for each atom in the inhibitors were determined at the B3LYP/6–31G level for a better understanding of the local reactivity of the tested inhibitor. The Fukui indices and local descriptors provide more complete information about the reactivity of the compounds under investigation and can help distinguish each portion of the inhibitor molecule based on its chemical activity with various substituent functional groups. As a result, the nucleophilic attack site will be where the value of $f^-$ is at its highest, whereas $f^+$ controls the site for electrophilic assault.

**Table 3: Selected Mulliken atomic charges and Fukui functions for DQP**

| Atoms | $q_k(N)$ | $q_k(N+1)$ | $q_k(N-1)$ | $f_k^+$ | $f_k^-$ | $\Delta f_k(r)$ | radical attack |
|---|---|---|---|---|---|---|---|
| **C1** | -0.135 | -0.147 | -0.119 | -0.012 | -0.016 | 0.004 | -0.014 |
| **C2** | -0.15 | -0.166 | -0.132 | -0.016 | -0.018 | 0.002 | -0.017 |
| **C3** | 0.287 | 0.272 | 0.299 | -0.015 | -0.012 | -0.003 | -0.0135 |
| **C4** | 0.287 | 0.272 | 0.299 | -0.015 | -0.012 | -0.003 | -0.0135 |
| **C5** | -0.15 | -0.166 | -0.132 | -0.016 | -0.018 | 0.002 | -0.017 |
| **C6** | -0.135 | -0.147 | -0.119 | -0.012 | -0.016 | 0.004 | -0.014 |
| **N2** | -0.571 | -0.618 | -0.538 | -0.047 | -0.033 | -0.014 | -0.04 |
| **C8** | 0.299 | 0.297 | 0.304 | -0.002 | -0.005 | 0.003 | -0.0035 |
| **C9** | 0.299 | 0.297 | 0.304 | -0.002 | -0.005 | 0.003 | -0.0035 |
| **N1** | -0.571 | -0.618 | -0.538 | -0.047 | -0.033 | -0.014 | -0.04 |
| **C11** | -0.238 | -0.276 | -0.188 | -0.038 | -0.05 | 0.012 | -0.044 |
| **C12** | 0.316 | 0.313 | 0.322 | -0.003 | -0.006 | 0.003 | -0.0045 |
| **C13** | 0.316 | 0.313 | 0.322 | -0.003 | -0.006 | 0.003 | -0.0045 |
| **C14** | -0.238 | -0.276 | -0.188 | -0.038 | -0.05 | 0.012 | -0.044 |
| **N4** | -0.598 | -0.633 | -0.578 | -0.035 | -0.02 | -0.015 | -0.0275 |
| **C16** | 0.258 | 0.227 | 0.28 | -0.031 | -0.022 | -0.009 | -0.0265 |
| **C17** | 0.258 | 0.227 | 0.28 | -0.031 | -0.022 | -0.009 | -0.0265 |
| **N3** | -0.598 | -0.633 | -0.578 | -0.035 | -0.02 | -0.015 | -0.0275 |
| **C19** | 0.064 | 0.064 | 0.072 | 0 | -0.008 | 0.008 | -0.004 |
| **C20** | 0.073 | 0.063 | 0.084 | -0.01 | -0.011 | 0.001 | -0.0105 |
| **C21** | 0.073 | 0.063 | 0.084 | -0.01 | -0.011 | 0.001 | -0.0105 |
| **C22** | 0.064 | 0.064 | 0.072 | 0 | -0.008 | 0.008 | -0.004 |
| **C23** | -0.208 | -0.212 | -0.2 | -0.004 | -0.008 | 0.004 | -0.006 |
| **C24** | -0.124 | -0.137 | -0.112 | -0.013 | -0.012 | -0.001 | -0.0125 |
| **C25** | -0.13 | -0.135 | -0.12 | -0.005 | -0.01 | 0.005 | -0.0075 |
| **C26** | -0.174 | -0.185 | -0.164 | -0.011 | -0.01 | -0.001 | -0.0105 |
| **C27** | -0.174 | -0.185 | -0.164 | -0.011 | -0.01 | -0.001 | -0.0105 |
| **C28** | -0.13 | -0.135 | -0.12 | -0.005 | -0.01 | 0.005 | -0.0075 |
| **C29** | -0.124 | -0.137 | -0.112 | -0.013 | -0.012 | -0.001 | -0.0125 |
| **C30** | -0.208 | -0.212 | -0.2 | -0.004 | -0.008 | 0.004 | -0.006 |

The Fukui function analysis (Table 3) identifies nitrogen atoms (N1–N4) and adjacent carbons (C11, C14) as nucleophilic centers (high $f^-$ values), indicating their propensity to donate electrons to electrophilic Fe atoms. For instance, N1 and N2 exhibit $f^-$ values of -0.033 and -0.018, respectively, aligning with their lone-pair availability for coordination. Conversely, low $f^+$ values across the molecule suggest limited susceptibility to electrophilic attack, reinforcing DQP's role as an electron donor. The moderate radical attack susceptibility at peripheral carbons (e.g., $C_{20}$, $C_{21}$) hints at secondary adsorption mechanisms,

such as radical stabilization or hydrogen bonding with surface hydroxyl groups. The electrostatic potential map (Figure 3) corroborates this, showing electron-rich regions (negative potential, red) localized over nitrogen atoms, which serve as anchoring points for Fe coordination. The pronounced negative potential at nitrogen atoms in electrostatic potential map visualizes nucleophilic centers, directly confirm Fukui function predictions. Generally, these findings highlight DQP's capacity for multidentate adsorption, where multiple active sites synergistically bind to the Fe surface, enhancing inhibition efficiency.

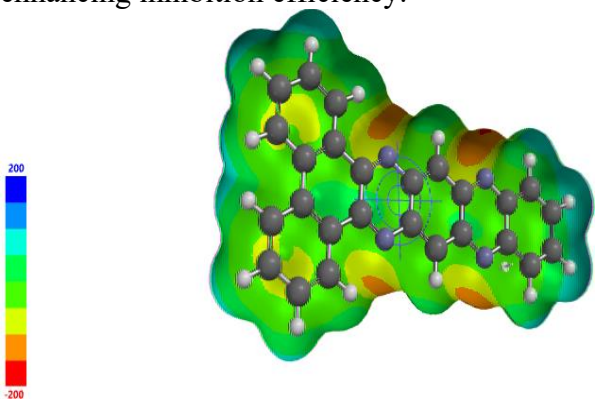


**Fig. 3: Molecular electrostatic potential (MEP) map of DQP**

### *3.4 Electronic Absorption Properties for Dibenzo [a,c[quinoxalino(2,3-i)phenazine (DQP)*

The vertical excitation energy maximum wavelength of absorption(nm) and, oscillator strengths (O.S) were determined. using TD-DFT for the transition from ground state of the molecules in gas phase with B3LYP at 6-31G** level of theory. Oscillator strength is a dimensionless quantity that expresses the relative strength of electronic transition. It determines the degree of sensitivity of a given atomic resonance. Its values are between 0 and 1. Values tending towards 1 indicates an allowed transition (Table 3). The ground state transition corresponds to excitation of electrons from HOMO to LUMO are presented in Table 4.38. The band assigned(nm) for: DQP correspond to the HOMO-LUMO transition and have Intra Charge Transfer (ICT) character with high possibility of n→ π* and π→π*, with average of high transition intensity. The calculated maximum wavelengths of absorption are in agreement with experimental absorption data in the Uv/visible region. The molecular orbital character corresponds to the energy difference (ΔE) between HOMO and LUMO, which determine the electronic transition from HOMO-LUMO. Compound DQP has the following calculated maximum wavelengths of absorption: 515.48 nm, 466.18 nm, 455.35 nm, 447.03 nm, 419.78 nm and, 377.71 nm. The lowesr absorption wavelength (377.71 nm), is assigned to n→ π*, the higher absorption wavelengths (419.78-466.18 nm) are assigned to π→ π*, while 515.48 nm is attributed to intramolecular charge transfer (ICT) from the donor part in HOMO to the acceptor end in LUMO transition as shown in **Table 3.** The intense transition at 419.78 nm (*f* = 0.6163) involves HOMO-2→LUMO (86%), indicative of charge-transfer processes critical for interfacial electron donation. These electronic properties not only facilitate adsorption but also stabilize the inhibitor-metal interface by redistributing charge density, thereby passivating the surface against oxidative attack.

**Table 3: Electronic transition data for Dibenzo [a,c[quinoxalino(2,3-i)phenazine**

| Maximum Absorption Wavelength(nm) | O.S (*f*) | Excitation Energy (eV) | Amplitude | Molecular Orbital/Character |
|---|---|---|---|---|
| **515.48** | 0.0380 | 2.4052 | 0.2154<br>0.9501 | HOMO-1→ LUMO<br>HOMO →LUMO (90%) |

| | | | | |
|---|---|---|---|---|
| **466.18** | 0.0013 | 2.6596 | 0.9749 | HOMO-3 → LUMO (95%) |
| **455.35** | 0.0015 | 2.7228 | 0.9745 | HOMO-4 → LUMO (95%) |
| **447.03** | 0.0001 | 2.7735 | 0.9636 | HOMO-1 → LUMO |
| **419.78** | 0.6163 | 2.9535 | 0.3530, 0.9256 | HOMO → LUMO, HOMO-2 →LUMO(86%) |
| **377.71** | 0.0074 | 3.2825 | 0.8761 | HOMO-5→LUMO (77%) |
| | | | 0.4492 | HOMO→ LUMO+1 |

### *3.5 Monte Carlo (MC) simulations*

The results of the MC stimulation studies showing the total energy of iron-inhibitor ($E_{Tot}$), adsorption energy ($E_{Ads}$), inflexible adsorption energy ($E_{Rigid}$) and the deformation energy ($E_{Def}$) of unwinding of the inhibitor particle on the Fe(110) surface are accounted for in Table 4. The absolute energy ($E_{Tot}$) of the substrate-adsorbate framework is connected with the steadiness and stability of the framework. The $E_{Tot}$ values show that the adsorption of compounds on Fe(110) surface is the thermodynamically stabilized. Likewise, low $E_{Ads}$ has been related areas of strength for with of the corrosion inhibitor on the metal surface (Khaled et al., 2009). The compound shows low adsorption energy. In addition, it was seen that relative stabilization of rigid adsorption energy of inhibitors contributed significantly to the bringing down of their adsorption energy. This suggests a stronger binding of these compounds to the iron surface, thereby retarding the corrosion process.

**Table 4 Monte Carlo simulation output for stable configurations of Fe(110)- QDP Inhibitor system (All energies are in kcal/mol)**

| System | $E_{Tot\ s}$ (kcal/mol) | $E_{Ads}$ (kcal/mol) | $E_{Rigid}$ (kcal/mol) | $E_{Def}$ (kcal/mol) |
|---|---|---|---|---|
| **Fe(110)-Inh A** | -13983.9 | -20131.0 | -14555.9 | -5575.0 |

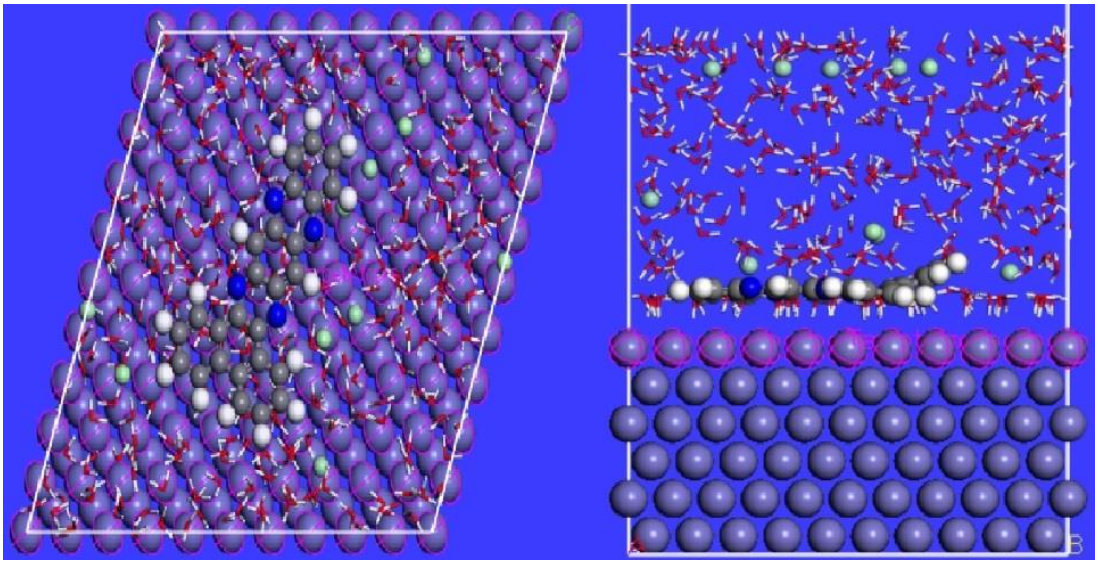

**Fig. 4: Monte Carlo simulation top and side views Adsorption of QDP on Fe(110)** surface

Fig. 4 shows the top and side perspectives on the adsorbed QDP inhibitors on Fe(110)

surface in aqueous solution. QDP molecules displayed good surface coverage on Fe(110). The simulated configuration (Figure 4) shows

DQP lies parallel to the Fe surface, maximizing π-orbital overlap and heteroatom interactions. Such orientation minimises surface energy and blocks active corrosion sites (e.g., kinks, vacancies), aligning with the planar geometry and electronic features discussed earlier. The negative ΔEback-donation values from DFT calculation imply that the inhibitors accept electrons via back donation; this is buttressed by the parallel arrangement of the compounds on Fe(110) via covalent and non-bonded interactions (Rahimi, et al., 2021; Oukhrib et al., 2021)

## 4.0 Conclusion

The study evaluated the corrosion-inhibiting potential of specific compounds through density functional theory (DFT) and Monte Carlo (MC) simulations. Computational analysis revealed advantageous electronic properties, including narrow energy gaps, reduced hardness, elevated electron affinity, and increased softness, suggesting strong reactivity. Fukui indices and molecular electrostatic potential (MESP) mapping identified molecular regions capable of dual electron interactions: donating electrons to metal d-orbitals and accepting electrons through back-donation. HOMO and LUMO visualizations highlighted asymmetric charge distribution, while MESP analysis showed carbon atoms as nucleophilic sites and heteroatoms as electrophilic targets. MC simulations demonstrated dense, stable adsorption of the compounds on Fe(110) surfaces, driven by covalent and nonbonded interactions, with molecular alignment parallel to the metal interface. DFT calculations supported these findings, showing negative $\Delta E_{back\text{-}donation}$ values that confirm electron-accepting behavior during back-donation. The combined results highlight the compounds' dual electronic functionality and robust adsorption as critical mechanisms for effective corrosion inhibition, emphasizing their potential as protective agents on iron surfaces.

## 5.0 References

Akinlosotu, O. M., Adejoro, I. A., Ogunyemi, B. T., & Adeleke, B. B. (2023). Synthesis, corrosion inhibition efficiency and adsorption behavior of dibenzo[a,c]quinoxalino(2,3-i)phenazine on mild steel in acidic medium. *American Journal of Agricultural Science, Engineering, and Technology, 7*(2). https://doi.org/10.54536/ajaset.v7i2.1063

Alao, A. O., Popoola, A. P., Dada, M. O., & Sanni, O. (2023). Utilization of green inhibitors as a sustainable corrosion control method for steel in petrochemical industries: A review. *Frontiers in Energy Research, 10*, 1063315. https://doi.org/10.3389/fenrg.2022.1063315

Anjum, A., Garg, R., Kashif, M., & Eddy, N. O. (2025). High-performance polymer nanocomposite coatings for enhanced and sustainable corrosion protection. *Inorganic Chemistry Communications*, **1***57*, 114411. https://doi.org/10.1016/j.inoche.2025.114411

Becke, A. D. (1993). Density-functional thermochemistry. III. The role of exact exchange. *The Journal of Chemical Physics, 98*(7), 5648–5652. https://doi.org/10.1063/1.464913

Belal, K., El-Askalany, A. H., Ghaith, E. A., & Salem Molouk, A. F. (2023). Novel synthesized triazole derivatives as effective corrosion inhibitors for carbon steel in 1M HCl solution: Experimental and computational studies. *Scientific Reports, 13*, 22180. https://doi.org/10.1038/s41598-023-49468-5.

Chang, Y. (2022). A Monte Carlo simulation of pitting corrosion of stainless steel. *Corrosion Science, 199*, 110176. https://doi.org/10.1016/j.corsci.2022.110176

Eddy, N. O,,Awe, F. E., Siaka, A., Magaji, L. & Ebenso, E. E. (2011). Chemical information from GC-MS studies of ethanol extract of *Andrographis paniculata*and their corrosion inhibition potentials on mild steel in HCl solution. *International Journal of Electrochemical Sciences 6,* 4316-4328

Eddy, N. O**.** (2010). Adsorption and inhibitive properties of ethanol extract of Garcinia kola and Cola nitida for the corrosion of mild steel in $H_2SO_4$. *Pigment and Resin Technology, 39* (6):347, https://doi.org/10.1108/03699421011085849353.

Eddy, N. O., Odiongenyi, A. O., Ebenso, E. E., & Garg, R. (2023). Plant wastes as alternative sources of sustainable and green corrosion inhibitors in different environments. *Corrosion Engineering, Science and Technology*. https://doi.org/10.1080/1478422X.2023.2204260

Eddy, N. O., Odoemelam, S. A., Ogoko, E. C. & Ita, B. I. (2010). Adsorption and inhibitive properties of Lincomycin for the corrosion of zinc in 0.01 – 0.05 M $H_2SO_4$. *Portugaliae Electrochimica Acta* 28(2), 73-85. doi: 10.4152/pea.201002073.

Eddy, N. O. (2010). Theoretical study on some amino acids and their potential activity as corrosion inhibitors for mild steel in HCl. *Molecular Simulation*. *35*(5), 354-363. DOI: 10.1080/08927020903483270

El Nemr, A., Elhebshi, A., Ashour, I., El Deab, M. S., Barghout, N. A., Eddy, N. O., & Ragab, S. (2024). Camphor tree bark extract as green corrosion inhibitor of LCS in 0.5 M $H_2SO_4$ with and without salt effect. *Journal of the Chinese Chemical Society*, **71**, 174–196. https://doi.org/10.1002/jccs.20230032

Elsayed, S. A., Barghout, N. A., Ragab, S., Abdel-Latif, E., Etman, H. A., Hamed, M. A., Eddy, N. O., & El Nemr, A. (2024). Condensed Fukui function and experimental evaluation of the corrosion inhibition properties of some antipyrinyl-imidazotriazole and their derivatives for copper in an acidic environment. *Journal of the Chinese Chemical Society*. https://doi.org/10.1002/jccs.202300351

Farhadian, A., Guo, L., & Neshati, J. (2021). Development of a novel thermally stable inhibitor based on furfuryl alcohol for mild steel corrosion in a 15% HCl medium for acidizing application. *Industrial & Engineering Chemistry Research, 60*(30), 11030–11044. https://doi.org/10.1021/acs.iecr.1c01946

Golubović-Bugarski, V., Petković, S., & Globočki-Lakić, G. (2021). The effect of corrosion on structural integrity and vehicle safety. *Mobility & Vehicle Mechanics, 47*(3), 49–62.

Halili, J., Jusufi, K., El Had, M. A., Bourzi, H., El Issami, S., Asmary, F. A., Parmar, V. S., & Len, C. (2021). DFT, Monte Carlo and molecular dynamics simulations for the prediction of corrosion inhibition efficiency of novel pyrazolylnucleosides on Cu(111) surface in acidic media. *Scientific Reports, 11*, 3771. https://doi.org/10.1038/s41598-021-82927-5

Kabanda, M. M., Obot, I. B., & Ebenso, E. E. (2013). Computational study of some amino acid derivatives as potential corrosion inhibitors for different metal surfaces and in different media. *International Journal of Electrochemical Science, 8*, 10839–10850.

Kalajahi, T. K., Mofradnia, S. R., Yazdian, F., Rasekh, B., & Nezhad, J. (2023). Computational evaluation of multifunctional nanostructured inhibitors

to control microbiologically influenced corrosion: DFT calculations and MD simulations. *Journal of Molecular Liquids, 367*, 120460. https://doi.org/10.1016/j.molliq.2022.120460

Khaled, K. F. (2009). Monte Carlo simulations of corrosion inhibition of mild steel in 0.5 M sulphuric acid by some green corrosion inhibitors. *Journal of Solid State Electrochemistry, 13*(11), 1743–1756. https://doi.org/10.1007/s10008-009-0845-y

Lee, C., Yang, W., & Parr, R. G. (1988). Development of the Colle-Salvetti correlation-energy formula into a functional of the electron density. *Physical Review B, 37*(2), 785–789. https://doi.org/10.1103/PhysRevB.37.785

Nahlé, A., Salim, R., El Hajjaji, F., Aouad, M. R., Messali, M., Ech-Chihbi, E., Hammouti, B., & Taleb, M. (2021). Novel triazole derivatives as ecological corrosion inhibitors for mild steel in 1.0 M HCl: Experimental & theoretical approach. *RSC Advances, 11*(7), 4147–4162. https://doi.org/10.1039/d0ra09679b.

Obot, I. B., Macdonald, D. D., & Gasem, Z. M. (2015). Density functional theory (DFT) as a powerful tool for designing new organic corrosion inhibitors: Part 1. *Corrosion Science, 99*, 1–30. https://doi.org/10.1016/j.corsci.2015.01.037

Odoemelam, S. A., Emeh, N. U., & Eddy, N. O. (2018). Experimental and computational chemistry studies on the removal of methylene blue and malachite green dyes from aqueous solution by neem (*Azadirachta indica*) leaves. *Journal of Taibah University for Science*, **12**(3), 255–265. https://doi.org/10.1080/16583655.2018.1465725.

Ogunyemi, B. T., Latona, D. F., & Adejoro, I. A. (2020). Molecular modeling and quantitative structure–property relationships (QSPRs) of purine derivatives as corrosion inhibitor in acid medium. *Scientific African, 8*, e00336, https://doi.org/10.1016/j.sciaf.2020.e00336

Ogunyemi, B. T., Latona, D. F., Ayinde, A. A., & Adejoro, I. A. (2020). Theoretical investigation into corrosion inhibition efficiency of some chloroquine derivatives using density functional theory. *Advance Journal of Chemistry Section A, 3*(4), 485–492.

Oukhrib, R., Abdellaoui, Y., Berisha, A., Abou Oualid, H., Halili, J., Jusufi, K., El Had, M. A., Bourzi, H., El Issami, S., Asmary, F. A., Parmar, V. S., & Len, C. (2021). DFT, Monte Carlo and molecular dynamics simulations for the prediction of corrosion inhibition efficiency of novel pyrazolylnucleosides on Cu(111) surface in acidic media. *Scientific Reports, 11*, 3771. https://doi.org/10.1038/s41598-021-82927-5

Oyeneyin, O. E., Ojo, N. D., Ipinloju, N., James, C. A., & Agbaffa, E. B. (2021). Investigation of corrosion inhibition potentials of some aminopyridine Schiff bases using density functional theory and Monte Carlo simulation. *Chemistry Africa, 5*, 319–332. https://doi.org/10.1007/s42250-021-00304-1

Parr, R. G., & Pearson, R. G. (1983). Absolute hardness: Companion parameter to absolute electronegativity. *Journal of the American Chemical Society, 105*(26), 7512–7516.

Parr, R. G., Szentpály, L. V., & Liu, S. (1999). Electrophilicity index. *Journal of the American Chemical Society, 121*(9), 1922–1924. https://doi.org/10.1021/ja983494x

Pearson, R. G. (1997). *Chemical hardness: Applications from molecules to solids*. Wiley-VCH.

Singaravelu, P., Anand, B., Loganathan, S., Eddy, N. O., & Garg, R. (2024). Experimental and theoretical investigations of the inhibition of the corrosion of mild steel in HCl by synthesized piperazine derivatives. *Protection of Metals and Physical Chemistry of Surfaces*, **60**(4), 777–794. https://doi.org/10.1134/S2070205124702034

Tomasi, J., Mennucci, B., & Cammi, R. (2005). Quantum mechanical continuum solvation models. *Chemical Reviews, 105*(8), 2999–3094. https://doi.org/10.1021/cr9904009

Verma, D. K., Kaya, S., Ech-chihbi, E., El-Hajjaji, F., Phukan, M. M., & Alnashiri, H. M. (2021). Investigations on some coumarin based corrosion inhibitors for mild steel in aqueous acidic medium: Electrochemical, surface morphological, density functional theory and Monte Carlo simulation approach. *Journal of Molecular Liquids, 329*, 115531. https://doi.org/10.1016/j.molliq.2021.115531

Wavefunction Inc. (2014). *Spartan '14*. Wavefunction Inc.

**Consent for publication**

Not applicable

**Availability of data**

The publisher has the right to make data public.

**Competing interests**

The authors declared no conflict of interest

**Ethical Consideration**

Not applicable

**Funding**

There is no source of external funding.

**Authors' contributions**

All components of this work were carried out by both authors